scientific reports

Check for updates

OPEN

Homologous relationship between FabG involved in fatty acid biosynthesis and SDR on chromosome II in the multi-chromosome pathogen *Vibrio anguillarum*

Dong-Gyun Kim[1,4], So Young Park[2,4], S. M. Rafiquzzaman[3] & Jong Min Lee[2]✉

Vibrio anguillarum **threatens fish and larval farming industries and human health worldwide. The identification of bacterial adaptation and responses to stress due to environmental changes is vital for establishing a response strategy for pathogenic *Vibrio*. Previously, short-chain dehydrogenase/reductase (SDR) was identified on chromosome II of the multichromosomal *V. anguillarum*. In this study, a comparison of SDR and the enzyme FabG-1b (encoded on chromosome I and responsible for the β-ketoacyl acyl carrier protein (ACP) reductase in fatty acid biosynthesis (FAS II)) showed that the amino acid sequence homology was only 33.2%; however, the core of functionality, which includes the NAD(P)-binding domain and the conserved region of the active site, the topologies predicted using sequence-based homology modeling, and the quaternary homotetramer-type structures showed a significant similarity. FabG-1b was specific to the substrates fluorinated and halogenated aliphatic ketones, aromatic ketones, and aromatic β-ketoesters and SDR toward non-fluorinated and non-halogenated aliphatic ketones, aromatic ketones, and non-aromatic β-ketoesters. This complementary catalytic efficiencies of the two enzymes on various substrates conclusively supports the hypothesis that the two enzymes are likely homologs. This is the first study to report potential paralogous enzymes FabG-1b and SDR in *Vibrio*. This information improves our understanding of bacterial FAS for establishing strategies to overcome infectious diseases caused by pathogenic strains and identify targets for developing new antibacterial agents.**

Keywords *Vibrio anguillarum*, Short-chain dehydrogenase/reductase (SDR), β-ketoacyl acyl carrier protein (ACP) reductase, FabG, Fatty acid biosynthesis, Paralogs

Vibrio genus comprises gram-negative bacteria belonging to > 206 species in the phylum Proteobacteria. The members of this genus are autochthonous and found in numerous aquatic environments, such as rivers, estuaries, oceans, and deep sea[1]. The majority of *Vibrio* species are non-pathogenic and are commonly found in healthy aquatic environments and aquatic organisms. However, certain species are pathogenic and can induce 'vibriosis,' predominantly affecting animals (e.g., *V. salmonicida* and *V. tubiashii*) or humans (e.g., *V. cholerae*, *V. vulnificus*, and *V. parahaemolyticus*), while others function as zoonotic pathogens (e.g., *V. damsela* and *V. harveyi*)[2–7]. Therefore, vibriosis is a major public health concern as it may cause severe illnesses in humans and animals with detrimental consequences[8,9]. *Vibrio anguillarum* causes hemorrhagic sepsis and threatens the survival of various marine, freshwater, and brackish water fishes, bivalves, and crustaceans, resulting in enormous economic damage to fish and larval farming industries worldwide owing to significant morbidity and mortality rates[10,11]. Hence, considerable research has been undertaken to elucidate its underlying pathogenic virulence mechanisms and

[1]Biotechnology Research Division, National Institute of Fisheries Science, Busan, Republic of Korea. [2]Department of Biotechnology, Pukyong National University, Busan 48513, Republic of Korea. [3]Department of Fisheries Biology and Aquatic Environment, BSMRAU, Gazipur, Bangladesh. [4]Dong-Gyun Kim and So Young Park contributed equally to this work. ✉email: jmlee84@pknu.ac.kr

develop rapid detection techniques and effective disease prevention strategies. Despite these efforts, not much is known regarding *V. anguillarum* especially compared with that of human pathogenic *Vibrio* spp., including *V. cholerae*, *V. parahaemolyticus*, and *V. vulnificus*[12–18].

Advances in sequencing techniques, equipment, and bioinformatics have revealed the presence of multi-chromosome systems in certain bacterial species. While our current understanding is insufficient to address the fundamental question regarding the origin of bacterial multi-chromosomes, it is known that the primary chromosome performs most housekeeping functions[19]. Moreover, the additional chromosome, believed to have evolved from a plasmid, is thought to serve as an alternative reservoir for newly acquired genes of largely unknown origin and function, as well as to maintain backups of specific essential genes[20,21]. In particular, *Vibrio* responds appropriately to stresses such as temperature, pH, salts, osmotic change, and nutrient starvation in the natural or systemic environment within the host and activates biofilm, quorum sensing, viable but nonculturable (VBNC), and resuscitation mechanisms for survival and prosperity. The multichromosomal system may be responsible for survival in this barren and rapidly changing environment and may have been selected as an evolutionary path to respond quickly and appropriately through chromosome evolution[19]. Therefore, the identification of bacterial adaptation and responses to stress due to environmental changes is vital for establishing a response strategy for pathogenic *Vibrio* as it would provide information on growth characteristics, infection mechanisms, and virulence factors.

Fatty acids are essential components of cell membrane phospholipids that form the permeability barrier and are responsible for molecular anchoring and energy conservation[22]. Bacterial fatty acid biosynthesis (FAS II) is catalyzed by individual enzymes with independent activities at each stage of phospholipid acyl chain production, unlike mammalian fatty acid biosynthesis (FAS I), which consists of multifunctional fatty acid synthases derived from a single gene[23]. Fatty acids in phospholipids determine membrane viscosity and play essential roles in membrane lipid homeostasis and survival in response to diverse environments such as the passive permeability of hydrophobic molecules, active solute transport, and protein–protein interactions[24,25]. Therefore, each enzyme essential for fatty acid synthesis is a potential target for the development of new antibacterial agents. In particular, β-ketoacyl-ACP reductase (FabG) is an enzyme involved in the reduction of the FAS II system. It reduces 3-ketoacyl-ACP to 3-hydroxyacyl-ACP, which is essential for the elongation of FAS II[24]. FabG is the only known isoenzyme of this type in bacteria and is highly conserved and ubiquitously expressed in bacteria. Therefore, it has been a key target in numerous attempts to develop new antibacterial agents[26,27].

FabG has long been recognized as a canonical member of the short-chain dehydrogenase/reductase (SDR) superfamily[28]. The common activity of this superfamily is to perform a wide range of reduction and dehydrogenation reactions involving the addition or removal of hydrogen from specific substrates in an NADPH-dependent manner. In our previous study, we already identified the SDR, which downregulated protein expression under stresses, on chromosome II of *V. anguillarum* NB10[29]. Because of its conserved amino acid sequence and protein structure homology, we hypothesized that FabG-1b and the SDR on each chromosome of *V. anguillarum* NB10 may play complementary roles in fatty acid synthesis. Therefore, in this study, FabG-1b on chromosome I was identified and compared the similarity in structure and enzymatic activity between the two enzymes. We believe that these results would provide important information for an in-depth understanding of the bacterial fatty acid synthesis process for establishing strategies to respond to infectious diseases caused by pathogenic strains.

Materials and methods

Media and reagents

The media used for the bacterial culture, namely, Brain Heart Infusion (BHI) and Luria–Bertani (LB), were provided by BD Difco (Becton Dickinson and Co., Sparks, MD, USA). All substrates and reagents such as acetoacetyl coenzyme A (AAC), ethyl acetoacetate (EAA), 2-heptanone (2H), 1,1,1-trifluoroacetone (1,1,1TFA), acetophenone (AP), 2′-chloroacetophenone (2′CAP), 4′-chloroacetophenone (4′CAP), 4′-fluoroacetophenone (4′FAP), ethyl 4-chloroacetoacetate (ECAA), ethyl benzoylacetate (EBA), and β-nicotinamide adenine dinucleotide 2′-phosphate reduced tetrasodium salt hydrate (NADPH) needed for determining enzyme activity were purchased from Sigma-Aldrich (St. Louis, MO, USA).

Bacterial strains, media, culture conditions, and plasmid

V. anguillarum NB10 (serotype O1) was used in this study[30]. *Escherichia coli* DH5α and *E. coli* BL21 (DE3) were used as host cells for constructing the recombinant plasmid and for protein expression, respectively. *V. anguillarum* NB10 was standard cultured in BHI media at 25 ℃ under aerobic conditions. The two *E. coli* strains were standard cultured at 180 rpm at 37 °C in LB media. Each strain was stored at -70 °C using 20% glycerol and 7% dimethyl sulfoxide (DMSO). The *E. coli* expression vector pET-22b(+) (Novagen, Madison, WI, USA) was used for the overexpression of the target proteins[31].

Genome analysis, and in silico screening for FAS II-related proteins

Genomic analysis of *V. anguillarum* NB10 was performed using the complete genome sequence deposited in the National Center for Biotechnology Information (NCBI; accession number: PRJEB5701)[32]. The circular map was constructed using the Proksee (https://proksee.ca/). Genomic annotation was performed using the RAST (Rapid Annotation using Subsystem Technology 2.0; https://rast.nmpdr.org/) and BV-BRC (Bacterial and Viral Bioinformatics Resource Center; https://www.bv-brc.org/) services, and all results were compared and analyzed to complete the annotation. General biological features of the subsystems were analyzed using the RAST server. Genes related to fatty acid biosynthesis were primary screened based on the annotated information of each coding sequence. Putative proteins primary annotated as hypothetical proteins were then compared to known enzymes in the bacterial FAS II system, and subsequently re-annotated by sequence homology analysis using

Basic Local Alignment Search Tool (BLAST). Furthermore, it was confirmed the essential proteins in FAS II through structure homology modeling and compared their structural homology with known FAS II-related proteins. The method of the three-dimensional (3D) structure modeling and the referenced protein database are provided in Sect. 2.4. The fatty acid synthesis pathway was verified by comparative analysis with the Genome and Kyoto Encyclopedia of Genes and Genomes (KEGG) pathway databases (https://www.genome.jp/kegg/)[33]. A phylogenetic tree of each gene and amino acid involved in fatty acid synthesis was constructed using MEGA 7.0 software (Molecular Evolutionary Genetics Analysis; https://www.megasoftware.net/). Phylogenetic distances were calculated according to the neighbor-joining method, using the Kimura two-parameter model, maximum-likelihood, and maximum-parsimony method[34–36]. The nucleotide sequence identity matrix and amino acid sequence homology of the fatty acid synthesis-related proteins were calculated using the BioEdit 7.2 program.

3D homology-modeling of protein and ligand and molecular docking

Tertiary structure prediction, modeling, visualization, and molecular docking of proteins and ligands generated based on the amino acid sequences of FabG-1b and SDR were performed as described in our previous studies[37,38]. For 3D structural modeling of each protein, homologous proteins were screened using the protein databases of AlphaFold (https://alphafold.ebi.ac.uk//), NCBI (https://www.ncbi.nlm.nih.gov/structure/), and RCSB (https://www.rcsb.org/), and candidate templates were selected for structural prediction. The amino acid sequences of FabG-1b and SDR were then applied to a protein structure homology modeling server (Swiss-Model; https://swissmodel.expasy.org/) to select templates whose structures were determined using X-ray crystallography[39]. The final predicted tertiary structures were constructed based on the selected templates. The crystal structures of 3-ketoacyl-(acyl carrier protein) reductase (PDB ID:3TZK) from *V. cholerae* and 2,3-butanediol dehydrogenase (PDB ID:6XEW) from *Serratia marcescens* were used as templates for FabG-1b and SDR, respectively. The 3D conformers of epigallocatechin gallate (PubChem CID:65,064) and macrolactin B (PubChem CID:76,309,372), which act as FabG-1b ligands, were visualized using the PubChem Chemical Molecules Database (https://pubchem.ncbi.nlm.nih.gov/). Intermolecular binding sites and affinities of proteins and ligands were predicted and evaluated using the AutoDock (https://autodock.scripps.edu/), CB-Dock2 (https://cadd.labshare.cn/cb-dock2/) and Swiss-Dock (http://www.swissdock.ch/) servers. Intramolecular interactions were evaluated using the Protein Interactions Calculator (https://crick.mbu.iisc.ernet.in/~PIC)[40–42]. The visualization and further analysis of the molecular complexes, including density maps, trajectories, and structure matching, were performed using the UCSF Chimera-1.16 (https://www.cgl.ucsf.edu/chimera) program.

Molecular gene cloning, expression, and purification of recombinant protein

The gene encoding FabG-1b and SDR were amplified from genomic DNA of *V. anguillarum* NB10 using gene-specific primer sets via polymerase chain reaction (PCR; TaKaRa, Kyoto, Japan). The forward and reverse primers for FabG-1b (VaFabG_fp; 5'-GGCCCATATGATGAACCTAGAAGGCAAAATT-3', VaFabG_rp; 5'-GGCCCTCGAGTACCATGTACATCCCGCCATT-3') and SDR (VaSDR_fp; 5'-GGCCCATATGATGAATGGTTTAACCCATAAA-3', VaSDR_rp; 5'-GGCCCTCGAGAACGATTTTAGGTTGGCCGTC-3') each contained NdeI and XhoI restriction enzyme sites (underlined), respectively. PCR was performed for 25 amplification cycles at 95 °C for 30 s, 58 °C for 30 s, and 72 °C for 30 s. The PCR products and the pET-22b(+)were digested with NdeI and XhoI restriction enzymes at 37 °C for 3 h each, and then ligated using T4 ligase (TaKaRa, Kyoto, Japan) at 4 °C for 12 h. The recombinant plasmid was transformed into *E. coli* DH5α by heat shock at 42 °C for 60 s and plated on LB agar containing ampicillin (50 μg/mL) to verify the recombinant plasmid via colony PCR using the gene-specific primer sets. Subsequently, the recombinant plasmid was purified using the Qiagen Plasmid Midi purification kit (Qiagen Inc., Valencia, CA, USA) and retransformed into *E. coli* BL21(DE3) using the heat shock. The confirmation of the final recombinant plasmid was validated through sequencing using the T7 promoter primer (5′-TAATACGACTCACTATAGGG-3′) and the T7 terminator primer (5′-GCTAGTTATTGCTCAGCGG-3′). Sequencing was performed on an Applied Biosystems model 3730XL (Applied Biosystems, Foster City, California, USA).

The recombinant protein expression and purification were assessed with reference to the previous report[13,31,38]. Briefly, each *E. coli* BL21 (DE3) cell containing the recombinant vector was grown at 37 °C in 500 mL of LB medium containing ampicillin (100 μg mL^{-1}) until the optical density at 600 nm (OD_{600}) reached 0.8. Protein expression was then induced by the addition of 1 mM isopropyl-β-d-thiogalactopyranoside (IPTG) to the culture for a further 6 h at 37 °C. The harvested cells by centrifugation were resuspended in 50 mM Tris–HCl (pH 8.0) for cell disruption by sonication (Sonics & Materials, Inc., Newtown, CT, USA). The resulting supernatants were applied into Ni–NTA column system (Thermo Fisher Scientific, Sunnyvale, CA, USA) for enzyme purification. The presence of purified recombinant enzymes FabG-1b and SDR were confirmed on 15% sodium dodecyl sulfate polyacrylamide gel electrophoresis (SDS-PAGE). Quantification of purified recombinant enzymes were determined by the Bradford assay[43].

β-ketoacyl-ACP reductase activity

A β-ketoacyl-ACP reductase assay was performed by measuring NADPH oxidation[44]. NADPH (0.3 mM) was added to 50 mM potassium phosphate buffer (pH 7.0 ± 0.2) containing 10 μg of purified FabG-1b or SDR. Then, 0.1–0.2 mM of the substrates AAC, EAA, 2H, 1,1,1TFA, AP, 2′CAP, 4′CAP, 4′FAP, ECAA, or EBA was added. The mixture was allowed to react at 30 °C for 5 min, and the OD_{340} was measured using an OPTIZEN POP UV–visible spectrophotometer (KLAB, Daejeon, Korea). All substrates and buffers except the enzyme were used after preincubation at 30 ℃ for 5 min. Enzyme activity was expressed as the difference in OD, which indicated the decrease in NADPH level. One unit of enzyme activity was defined as the amount of protein that produced 1 μmol of NADPH per minute. The enzyme kinetic parameters of FabG-1b and SDR were determined under conditions of 30 °C, pH 7 ± 0.2, and 5 min. The reaction velocity was measured at substrate concentrations in the

range of 0–1.0 mmol. The data were analyzed using double-reciprocal plots (Lineweaver–Burk plots). The molar extinction coefficient for NADPH at 340 nm was 6.22 L $mmol^{-1}$ cm^{-1}. All kinetic parameters presented in this study are mean values derived from triplicate measurements.

Statistical analysis

All data were analyzed using one-way analysis of variance (ANOVA) with the Statistical Package for the Social Sciences (SPSS), followed by Duncan's multiple range test. Statistical significance was accepted at $p < 0.05$, unless otherwise noted.

Results

Genomic features of *V. anguillarum* NB10 and gene locus related to fatty acid biosynthesis and SDR

Genome analysis was performed to understand the multi-chromosome system of *V. anguillarum* NB10. Figure 1 shows the general genomic characteristics of *V. anguillarum* NB10 and the gene locus related to fatty acid biosynthesis and SDR. *V. anguillarum* NB10 is a multi-chromosome bacteria harboring chromosome I (3.12 Mbp), chromosome II (1.12 Mbp), and one plasmid (67 Kbp) (Fig. 1a). Chromosome I houses 2,704 protein coding sequences, 25 rRNAs, and 89 tRNAs with a GC mol % of 44.7%. Chromosome II housed 1,014 protein coding sequences and four tRNAs with a GC mol % of 44.6%. The plasmid housed 58 protein-coding sequences (Fig. 1b). Analysis of the genes on chromosome I annotated in the subsystems showed that 224 functional genes related to amino acid metabolism (biosynthesis and degradation), constituted the highest proportion of the genes, followed by 161 genes related to protein metabolism (biosynthesis, degradation, folding, peptidyl-prolyl *cis–trans* isomerase, chaperones, processing and modification, and periplasmic disulfide interchange) (Fig. 1c and d). On chromosome II, 46 genes were involved in carbohydrate metabolism, accounting for the highest proportion of functional genes, followed by 21 for amino acid metabolism. Four genes related to aromatic amino acid synthesis were detected on the plasmid.

The fatty acid biosynthesis system of *V. anguillarum* NB10 housed the *fabH-fabD-fabG-acp-fabF* cluster observed in a typical bacterial FAS II system (Fig. 1e). Moreover, individual *fabL*, *fabA*, *fabZ*, and *fabB* genes, which encode key enzymes involved in fatty acid elongation and β-ketoacyl synthesis in the FAS II system, and extra partial *fabH*, *fabA*, *fabG*, and *fabF* clusters were observed at each locus. In contrast, *sdr* was presumed to exist as a single gene rather than as a cluster on chromosome II (Fig. 1f).

Genetic organization of the FAS II of *V. anguillarum* NB10

Proteins presumed to be essential enzymes in the fatty acid biosynthetic pathway were selected as queries and reannotated based on the latest BLAST database and protein structure comparisons (Table 1). Figure 2 shows the proposed mechanism of fatty acid biosynthesis of *V. anguillarum* NB10 according to the reannotated result and the putative products generated from the reaction hierarchy. FabH1 (protein ID CDQ50748.1) as a β-ketoacyl-ACP synthase III catalyzes the production of β-ketoacyl-ACP through a condensation reaction using malonyl-ACP converted from malonyl-CoA by FabD (CDQ50747.1; malonyl CoA-ACP transacylase). FabH1 catalyzes the generation of β-ketoacyl-ACP through straight-chain fatty acid synthesis using acetyl-CoA as the precursor. The generated β-ketoacyl-ACP is reduced to β-hydroxyacyl-ACP by FabG-1b (CDQ50746.1; 3-ketoacyl-ACP reductase) and then dehydrated to *trans*-2-enoyl-ACP by FabZ (CDQ50948.1; β-hydroxyacyl-ACP dehydratase). Subsequently, *trans*-2-enoyl-ACP is reduced to acyl-ACP by FabL (CDQ49856.1, enoyl-ACP reductase). Acyl-ACP is synthesized in the form of β-ketoacyl-ACP by β-ketoacyl synthase (FabF-1b; CDQ50744.1, or FabB; CDQ50829.1), which is then elongated during fatty acid synthesis. Acyl-ACP of an appropriate length is used for phospholipid biosynthesis, whereas β-hydroxyacyl-ACP of an appropriate length is used as a component of lipid A in lipopolysaccharides. The *trans*-2-enoyl-ACP can be used in unsaturated fatty acid biosynthesis. FabA-1a (CDQ50678.1; β-hydroxydecanoyl-ACP dehydratase) as a dual catalytic enzyme dehydratases 3-hydroxydecanoyl-ACP to *trans*-2-decenoyl-ACP and subsequently isomerizes to cis-3-decenoyl-ACP. The *cis*-3-decenoyl-ACP is used as a substrate for FabB (CDQ50829.1; 3-ketoacyl-ACP synthase) able to continue with the next fatty acid elongation step maintaining the double bond. In addition to the FabA/B pathway for unsaturated fatty acid synthesis, there is a DesA (CDQ50217.1; fatty acid hydroxylase family sterol desaturase) that introduces a double bond at carbon 9 of the carbon chain, which is the oxidative unsaturated system of existing fatty acids. Therefore, the fatty acid synthesis of *V. anguillarum* NB10 mainly involves the condensation and initiation of fatty acid synthesis by the synthesis catalyst fabH; fatty acid elongation through a series of reduction and dehydration catalysts FabG, FabZ (FabA), and FabL; and the recycling of fatty acids by FabF (FabB).

Sequence homolog relationship between SDR and FabG-1b

Phylogenetic analysis based on the amino acid sequence of SDR on chromosome II confirmed that it belongs to the FabG category, which acts as a 3-ketoacyl-ACP reductase in the bacterial FAS II system (Fig. 3a). Additionally, maximum-parsimony, maximum-likelihood, and neighbor joining algorithms showed that SDR formed a single clade with two FabGs, namely, FabG-1b and FabG-1a, on chromosome I. Sequence homology analysis between SDR and FAS II-related enzymes showed that the highest sequence similarity existed between SDR and FabG-1b, which formed the *fabH-fabD-fabG-acp-fabF* cluster; we detected 44.0% nucleotide identity and 33.2% amino acid similarity (Fig. 3b). Moreover, the alignment of the amino acid sequences between SDR and FabG-1b revealed the conserved motifs Thr-Xaa_3-Gly, which is an NAD(P) coenzyme-binding site, and Ser-Xaa_{12}-Tyr-Xaa_3-Lys, which is an active site containing a Tyr residue, in both enzymes (Fig. 3c).

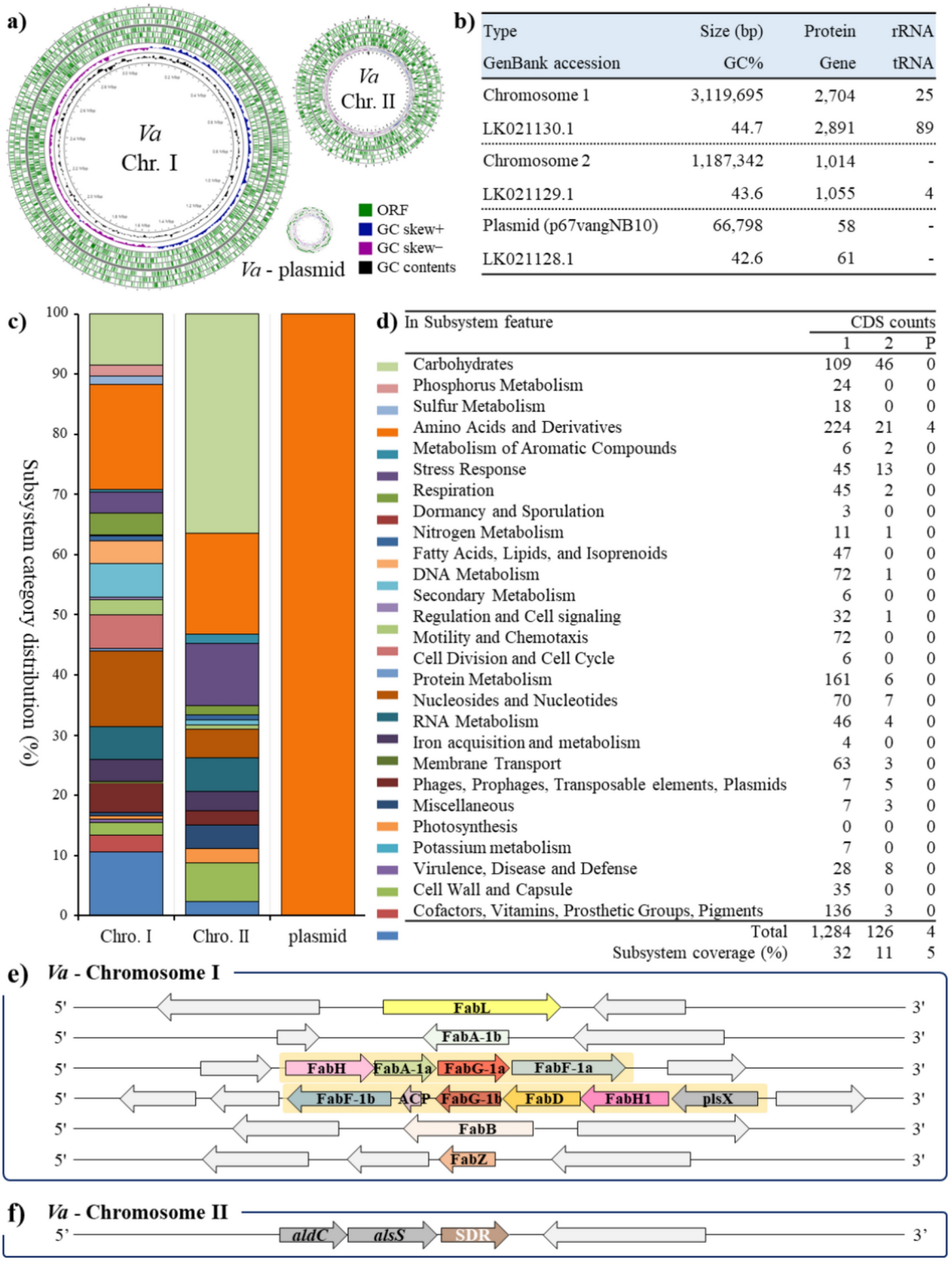

b)

Type	Size (bp)	Protein	rRNA
GenBank accession	GC%	Gene	tRNA
Chromosome 1	3,119,695	2,704	25
LK021130.1	44.7	2,891	89
Chromosome 2	1,187,342	1,014	-
LK021129.1	43.6	1,055	4
Plasmid (p67vangNB10)	66,798	58	-
LK021128.1	42.6	61	-

d)

In Subsystem feature	CDS counts 1	2	P
Carbohydrates	109	46	0
Phosphorus Metabolism	24	0	0
Sulfur Metabolism	18	0	0
Amino Acids and Derivatives	224	21	4
Metabolism of Aromatic Compounds	6	2	0
Stress Response	45	13	0
Respiration	45	2	0
Dormancy and Sporulation	3	0	0
Nitrogen Metabolism	11	1	0
Fatty Acids, Lipids, and Isoprenoids	47	0	0
DNA Metabolism	72	1	0
Secondary Metabolism	6	0	0
Regulation and Cell signaling	32	1	0
Motility and Chemotaxis	72	0	0
Cell Division and Cell Cycle	6	0	0
Protein Metabolism	161	6	0
Nucleosides and Nucleotides	70	7	0
RNA Metabolism	46	4	0
Iron acquisition and metabolism	4	0	0
Membrane Transport	63	3	0
Phages, Prophages, Transposable elements, Plasmids	7	5	0
Miscellaneous	7	3	0
Photosynthesis	0	0	0
Potassium metabolism	7	0	0
Virulence, Disease and Defense	28	8	0
Cell Wall and Capsule	35	0	0
Cofactors, Vitamins, Prosthetic Groups, Pigments	136	3	0
Total	1,284	126	4
Subsystem coverage (%)	32	11	5

Fig. 1. Genomic features of the *V. anguillarum* NB10. (**a**) Circular plot of the genomes of chromosome I and II and the plasmid. b) General genomic features. (**c**–**d**) Subsystem category distribution and subsystem feature counts. (**e**–**f**) Gene organization of the FAS II in multi-chromosome. (**e**–**f**) gene organization of the FAS II and SDR in multi-chromosome. Chr.; Chromosome.

Systematic comparison between SDR and FabG-1b using in silico structural modeling

The sequence-based quaternary structural models of SDR and FabG-1b are shown in Fig. 3d–k. Both proteins formed a homotetrameric quaternary structure with the subunit chains A, B, C, and D. The superimposition of the two proteins showed a significantly similar three-dimensional arrangement in each conserved region

CDS locus	Gene	Locus_tag	Product	Protein_ID
1,062,830. 1,063,588	*sdr*	Chromosomal II VANGNB10_ cII0928	(EC -.-.-.-) short-chain dehydrogenase/reductase	CDQ48825.1
1,118,724. 1,120,727	*fadH* (*fabL*)	Chromosomal I VANGNB10_ cI0942	(EC 1.3.1.34) 2,4-dienoyl-CoA reductase	CDQ49856.1
1,500,571. 1,501,089	*fabA* (*fabA-1b*)	Chromosomal I VANGNB10_ cI1267c	(EC 4.2.1.59) 3-hydroxydecanoyl-[ACP] dehydratase	CDQ50181.1
2,070,034. 2,071,137	ND (*fabH*)	Chromosomal I VANGNB10_ cI1765	(EC 2.3.1.180) β-ketoacyl-[ACP] synthase	CDQ50677.1
2,071,115. 2,071,579	ND (*fabA-1a*)	Chromosomal I VANGNB10_ cI1766	(EC 4.2.1.-) putative β-hydroxydecanoyl-[ACP] dehydratase	CDQ50678.1
2,071,576. 2,072,301	*fabG-1a*	Chromosomal I VANGNB10_ cI1767	(EC 1.1.1.100) Glucose/ribitol dehydrogenase	CDQ50679.1
2,072,298. 2,073,527	*fabF-1a*	Chromosomal I VANGNB10_ cI1768	(EC 2.3.1.41) 3-oxoacyl-[ACP] synthase 2; β-ketoacyl synthase	CDQ50680.1
2,142,536. 2,143,786	*fabF-1b*	Chromosomal I VANGNB10_ cI1832c	(EC 2.3.1.41) 3-oxoacyl-[ACP] synthase 2	CDQ50744.1
2,143,871. 2,144,185	*acp*	Chromosomal I VANGNB10_ cI1833c	(EC -.-.-.-) Acyl carrier protein	CDQ50745.1
2,144,339. 2,145,076	*fabG-1b*	Chromosomal I VANGNB10_ cI1834c	(EC 1.1.1.100) 3-oxoacyl-[ACP] reductase	CDQ50746.1
2,145,093. 2,146,016	*fabD*	Chromosomal I VANGNB10_ cI1835c	(EC 2.3.1.39) Malonyl CoA-[ACP] transacylase	CDQ50747.1
2,146,080. 2,147,030	*fabH1*	Chromosomal I VANGNB10_ cI1836c	(EC 2.3.1.180) 3-oxoacyl-[ACP] synthase 3	CDQ50748.1
2,147,036. 2,148,061	*plsX*	Chromosomal I VANGNB10_ cI1837c	(EC -.-.-.-) fatty acid/phospholipid synthesis protein PlsX	CDQ50749.1
2,236,691. 2,237,902	*fabB*	Chromosomal I VANGNB10_ cI1917c	(EC 2.3.1.41) 3-ketoacyl-[ACP] synthase	CDQ50829.1
2,358,552. 2,358,983	*fabZ*	Chromosomal I VANGNB10_ cI2036c	(EC -.-.-.-) (3R)-hydroxymyristoyl-[ACP]-dehydratase	CDQ50948.1

Table 1. short-chain dehydrogenase/reductase (SDR) and fatty acid biosynthesis (FAS II) related genes in the *V. anguillarum* NB10 genome.

(Fig. 3d and e). The secondary structures of the monomers FabG-1b and SDR contained seven major helices and strands, respectively (Fig. 3f and g). The seven α-helical elements forming the coenzyme binding pocket in helix α5 and catalytic active site in helix α1 were wrapped around central β-sheet consist of 3–2–1–4–5–6–7 topology. In addition, although the characteristics of individual amino acids constituting FabG-1b and SDR were different, the surface quaternary structure, including that of the coenzyme binding pocket and active site, showed a significantly similar structure except in helix α5 (Fig. 3h–k).

In Silico investigation of FabG-1b and SDR interactions with epigallocatechin gallate and macrolactin B inhibitors.

To infer the homology of the two proteins, we compared the homology of the domains containing the coenzyme-binding pocket and active site, which are responsible for their physiological functionality. The homology between SDR and the functional domains of FabG-1b was compared using in silico molecular docking analysis with the ligands epigallocatechin gallate and macrolactin B, which are known FabG inhibitors[45,46]. Epigallocatechin gallate was predicted to act as an inhibitor through chemical interactions with the residues Gly13-Ala14-Ser15-Arg16-Gly17-Ile18-Gly19 and Thr12-Gly13-Ala14-Arg16-Gly17-Ile18-Gly19-Arg20, which are present in the NAD(P)-binding pocket adjacent to the active sites of SDR and FabG-1b, respectively (Fig. 4a–b). Similar to the mode of action of epigallocatechin gallate, macrolactin B has also been predicted to act as an inhibitor by interacting with Thr12-Gly13-Ala14-Ala15-Asn16-Gly17-Gly19 and Thr12-Gly13-Asn16-Gly17-Ile18-Gly19, which are present in the NAD(P)-binding pocket of each SDR and FabG-1b, respectively, (Fig. 4c and d). Therefore, in silico analysis showed that SDR on chromosome II and FabG-1b on chromosome I showed potential as FabG homologues based on similarity in sequences, structures, and active sites.

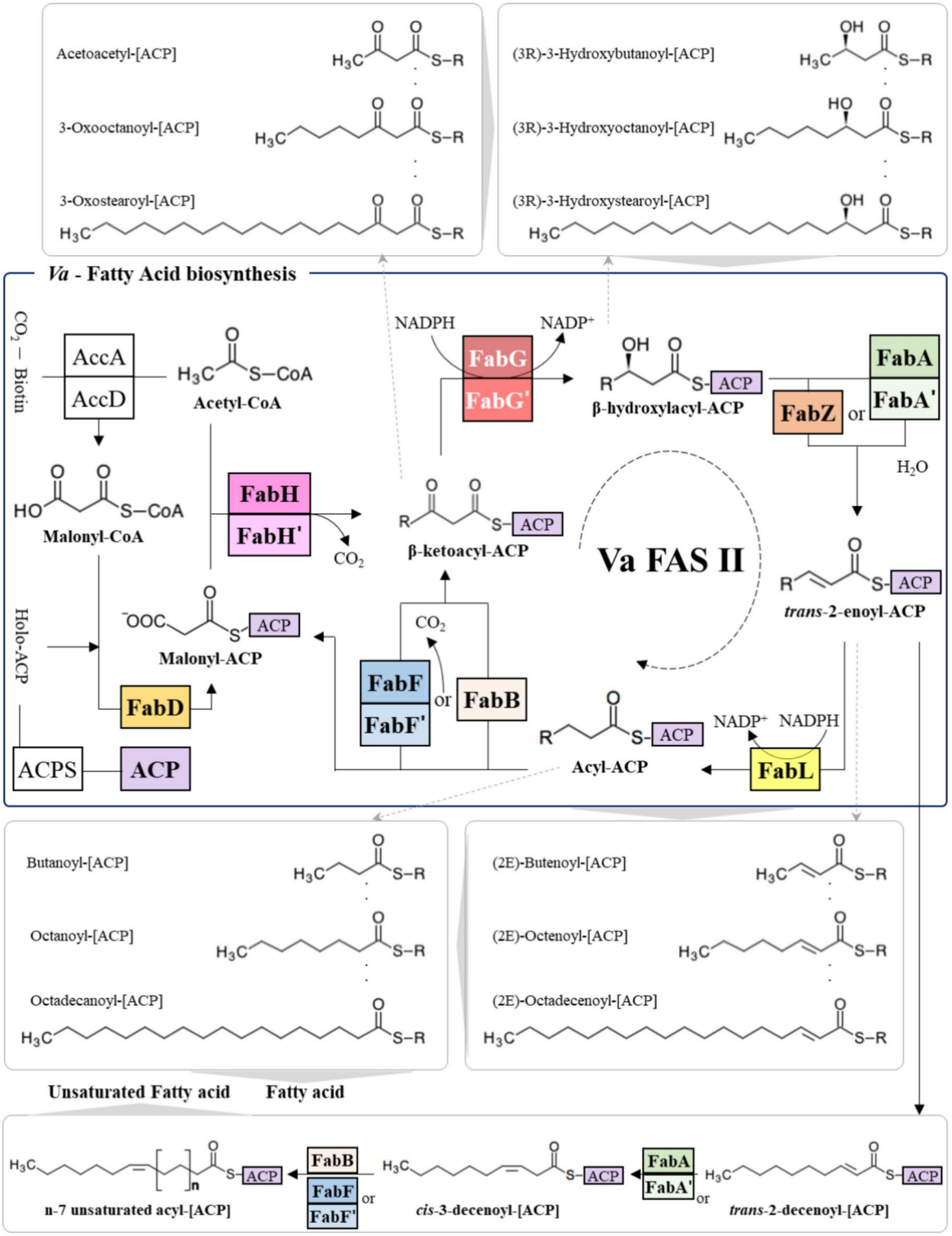

Fig. 2. The fatty acid biosynthesis mechanism of the *V. anguillarum* NB10 proposed through genome analysis and putative general compounds produced in reaction hierarchy.

Recombinant protein expression and enzyme kinetics of FabG-1b and SDR

Enzyme kinetic analysis was performed using proteomics and genome mining to prove the homologous relationship between FabG-1b and SDR. The two recombinant proteins, FabG-1b and SDR, were overexpressed in *E. coli* and purified using Ni–NTA His-binding resin. Both FabG-1b and SDR were overexpressed in the soluble fraction of the cell extracts, and the two purified recombinant proteins showed a clear single band on SDS-PAGE, confirming that they were effectively purified (Fig. S1).

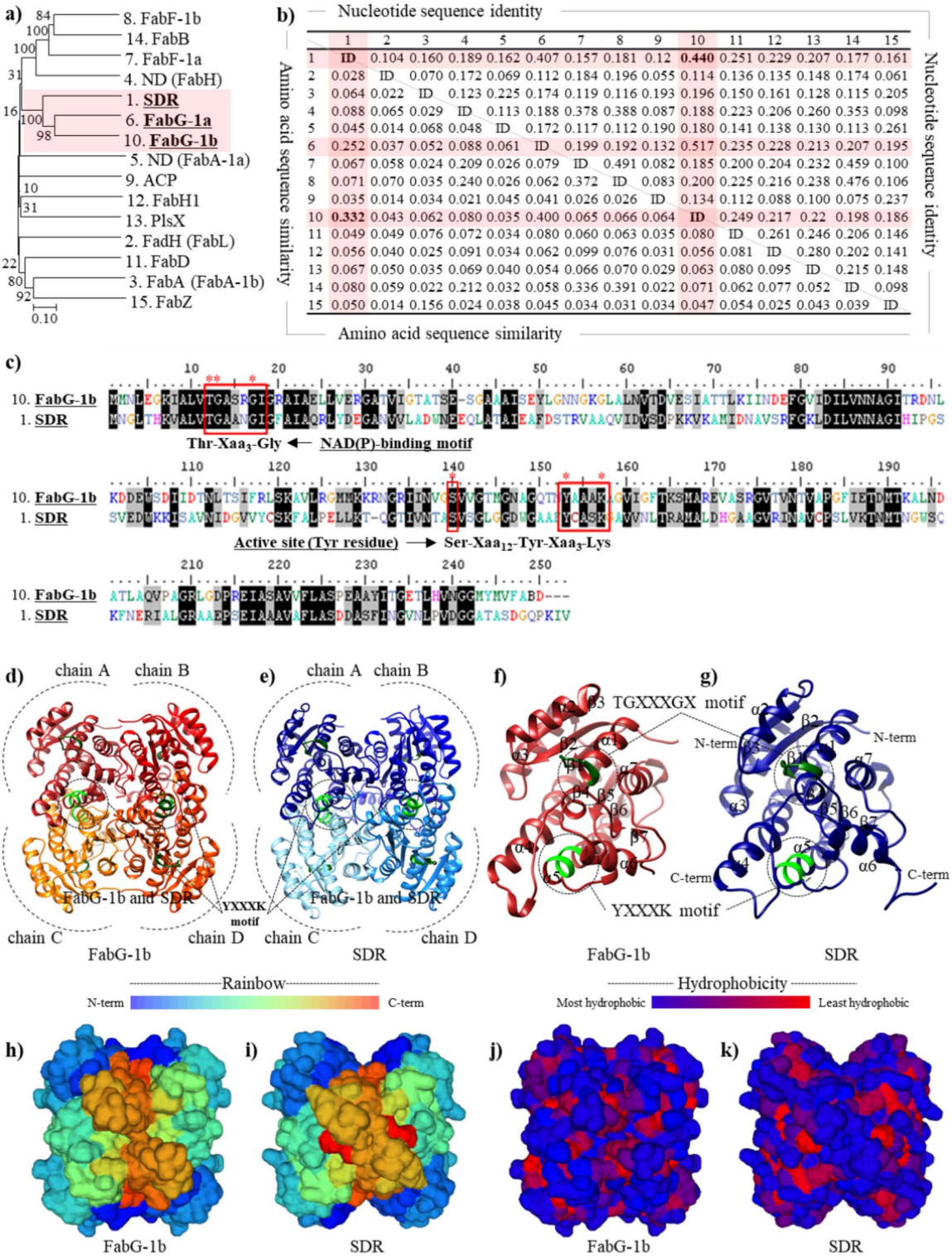

To compare the activities of the two enzymes with respect to the substrate, enzyme kinetics were calculated using various ketones (Fig. 5). The catalytic efficiencies of FabG-1b and SDR for AAC were 18.87 ± 0.94 and 19.61 ± 0.98, respectively, with no significant difference (Fig. 5a). For the EAA substrate, the catalytic efficiencies were 33.33 ± 1.61 for FabG-1b and 50.01 ± 2.50 for SDR, with SDR exhibiting approximately 1.5 times higher catalytic efficiency than FabG-1b (Fig. 5b). In the case of FabG-1b, its activity toward aliphatic ketones such as 2H and 1,1,1TFA showed significantly higher catalytic efficiency than towards aromatic ketones such as AP, 2'CAP, 4'CAP, and 4'FAP (Fig. 5c–h). Among aliphatic ketones, the catalytic efficiency for 1,1,1TFA (52.46 ± 4.55 10^{-3} mL min^{-1} mg^{-1}) fluorinated on the side chain showed significantly higher catalytic efficiency than toward 2H (40.36 ± 0.95). The catalytic efficiencies of halogenated (2'CAP; 27.85 ± 0.25 and 4'CAP; 28.12 ± 1.51) and fluorinated ketones (4'FAP; 17.74 ± 0.21) were approximately 1.21–2.48 times higher than that of AP (14.65 ± 0.65). The catalytic efficiency of halogenated ketone (4'CAP) was approximately twice as high as that of

◀**Fig. 3**. Comparative sequence analysis and predicted protein structure schematic of FabG and SDR. (**a**) Neighbor-joining phylogenetic tree based on amino acid sequences showing the relationships of FAS II related enzyme with FabG and SDR. The phylogenetic trees calculated by the neighbor-joining, maximum-likelihood, and maximum-parsimony methods were all consistent, with the tree based on the NJ method being presented as a representative. Bootstrap percentages based on 1,000 resamplings are shown at the nodes. Bar, 0.10 substitutions per amino acid position. (**b**) Sequence identity matrix of nucleotide and amino acid sequences from FAS II related enzymes in the *V. anguillarum* NB10. 1; SDR, 2; FadH (FabL), 3; FabA (FabA-1b), 4; ND (FabH), 5; ND (FabA-1a), 6; FabG-1a, 7; FabF-1a, 8; FabF-1b, 9; ACP, 10; FabG-1b, 11; FabD, 12; FabH1, 13; PLSX, 14; FabB, and 15; FabZ. (**c**) Comparison of amino acid sequences of FabG-1b and SDR. The red asterisk indicates conserved residues. (**d** and **e**) Schematic of helices and strands in homo tetramer form of FabG-1b and SDR. (**f**) and (**g**) Topology of the monomers composing each protein. (**h**–**k**) Protein quaternary structure of FabG-1b (**h** and **j**) and SDR (**i** and **k**) indicated according to each amino acid characteristics, amino acid strand and hydrophobicity.

fluorinated ketone (4'FAP), and the catalytic efficiency when the ketone was halogenated at 4' was 1.3-fold higher than when halogenated at 2', although the same ketones were halogenated. Additionally, FabG-1b was shown to exhibit similar substrate affinity for ECAA ($1.05 \pm 0.14\ 10^{-2}$ mg mL^{-1}) and EBA (1.09 ± 0.16) but the catalytic efficiency for EBA (33.41 ± 2.96) was about 1.4 times higher than that for ECAA (24.44 ± 0.04) owing to the differences in turnover number between that of ECAA ($2.54 \pm 0.13\ 10^{-2}$ min^{-1}) and EBA (3.63 ± 0.21) (Fig. 5i–j).

In contrast, SDR showed significantly higher catalytic efficiency for aliphatic ketones than for aromatic ketones, which is similar to that observed for FabG-1b but different from that of FabG-1b depending on the bound residues. Among aliphatic ketones, the catalytic efficiency of 2H (40.36 ± 0.96) was approximately 1.2 times higher than that of 1,1,1TFA (36.72 ± 0.53) fluorinated on the side chain. Moreover, the catalytic efficiency of 2H was 1.5 times higher than that of FabG-1b (Fig. 5c and d). SDR was observed to have significantly higher catalytic efficiency for halogenated (2'CAP; 24.34 ± 1.69 and 4'CAP; 28.12 ± 1.52) ketones than for AP (18.87 ± 1.96) and fluorinated ketone (4'FAP; 7.03 ± 0.23) in aromatic ketones (Fig. 5e–h). However, catalytic efficiency the activity of SDR on AP was approximately 3.0 times higher than that of FabG-1b owing to its higher substrate affinity. The catalytic efficiency of SDR for β-ketoesters were 41.58 ± 2.88 and 1.47 ± 0.26 for ECAA and EBA, respectively, which showed significant difference in activity (Fig. 5i–j). In particular, the activity of SDR against ECAA showed approximately 1.84 times higher catalytic efficiency that that against EBA owing to 1.87 times higher turnover than that of FabG-1b.

Therefore, FabG-1b showed higher catalytic efficiency for the substrates 1,1,1TFA, 2'CAP, 4'CAP, 4'FAP, and EBA, and SDR showed higher catalytic efficiency for EAA, 2H, AP, and ECAA. Furthermore, no significant differences were observed in the catalytic efficiencies of the two enzymes for AAC.

Discussion

Changes in the water environment parameters such as temperature, salinity, and organic carbon cycle directly affect the distribution, proliferation, and pathogenicity of *Vibrio*[47,48]. Owing to climate change, *Vibrio* contamination or infection tend to occur at accelerated rates regardless of the season[49]. Consequently, *Vibrio* infection has emerged as a serious social problem, owing to the enormous damage it causes to aquatic products that are an important protein source for humans in terms of food security and increasing the number of patients infected with *Vibrio*[50].

In addition to *V. anuillarum*, a variety of other *Vibrio* spp., namely, *V. alginolyticus*, *V. campbellii*, *V. cincinnatiensis*, *V. coralliilyticus*, *V. fluvialis*, *V. furnissii*, *V. hollisae*, *V. metschnikovii*, *V. mediterranei*, *V. mimicus*, *V. navarrensis*, *V. ordalii*, *V. proteolyticus*, and *V. splendidus* are potential opportunistic pathogens in humans[51–59]. Up to 10% of vibriosis cases reported each year originate from the non-agglutinating vibrios that were recognized as non-pathogenic species[60]. In particular, *V. alginolyticus* represents the marine microbiota and is a major fish pathogen that is generally not recognized as zoonotic. However, it has gradually been recognized as a causative agent of food poisoning and bloodstream and soft tissue infections in humans[61]. Moreover, rising ocean temperatures worldwide have led to the emergence of the environmental bacterium *V. fluvialis* as a human pathogen[62]. As climate warming continues, opportunistic species widely distributed in aquatic environments are increasingly being recognized as virulent human pathogens. Therefore, to overcome the negative impacts of *Vibrio* spp. and prevent their spread to local communities, continuous monitoring, tracking, prevention, and management of changes in *Vibrio* proliferation in marine environments and aquatic products are required[63]. However, tracking opportunistic *Vibrio* in aquatic products that are distributed in the consumption market, rapid quarantine and disinfection, and prevention of *Vibrio* contamination are limited by our current knowledge. Therefore, extensive biochemical research on opportunistic *Vibrio* species is needed to accumulate basic scientific information.

In our previous study, proteomic analysis of *V. anguillarum* was performed under temperature (15 °C and 37 °C), pH (5 and 10) and salt (2 M NaCl) stress conditions[29]. In brief, the upregulated protein expression was compared with those at normal growth conditions: deoxyribose-phosphate aldolase under low-temperature stress, threonine dehydratase under high-pH stress, and deoxyribose-phosphate aldolase, threonine dehydratase and transcriptional regulator under low-pH stress. In contrast, the protein expression of SDR was significantly downregulated under all the tested stress conditions. In the protein spot density-based expression rate analysis, SDR showed an expression rate of approximately 52.1% under high salinity stress conditions and < 50% under other stress conditions compared with that under normal conditions. Therefore, SDR, which is sensitive to various environmental conditions, was considered a suitable satellite marker for determining the stress conditions of *V.*

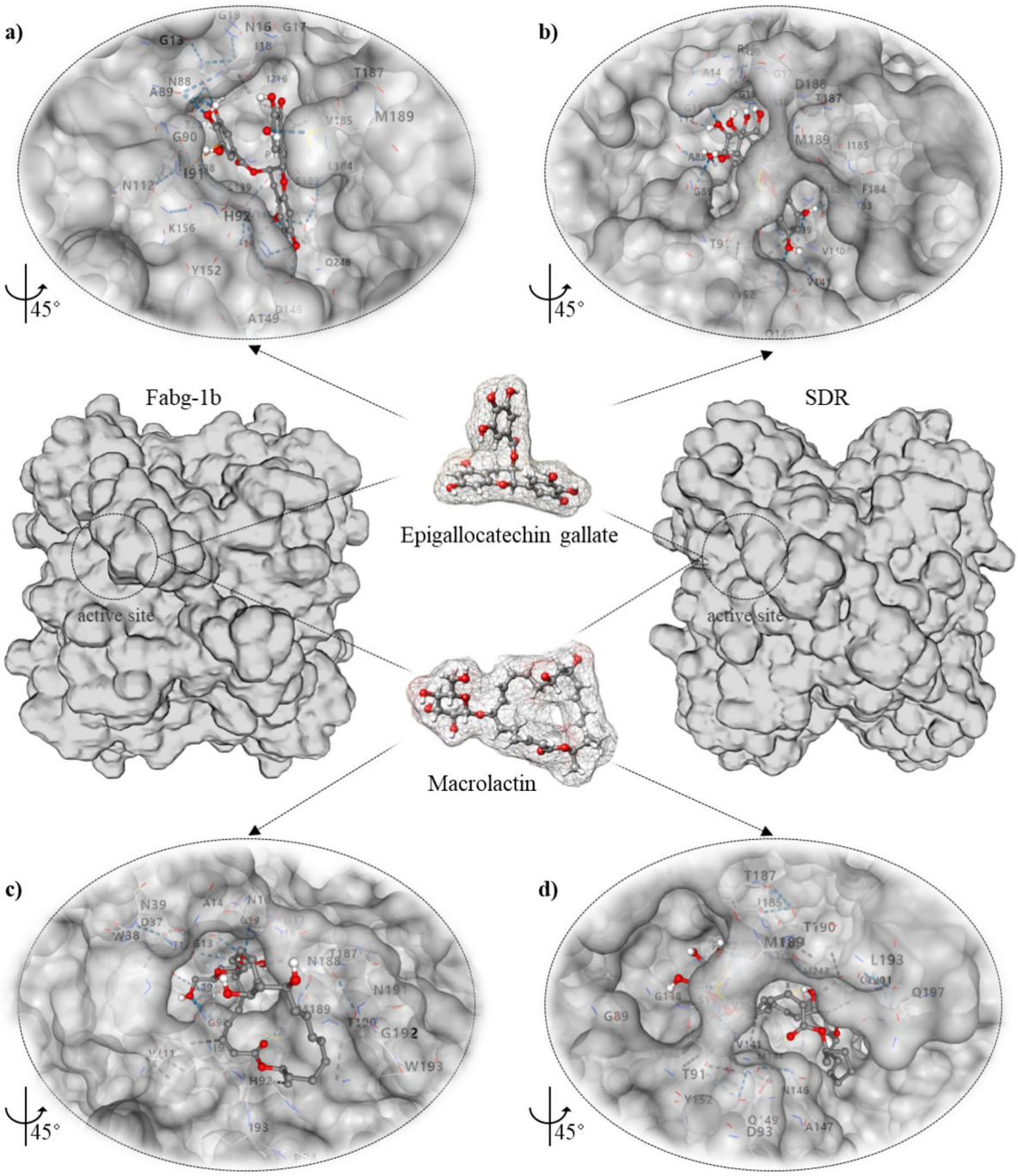

Fig. 4. Schematic of epigallocatechin gallate and macrolactin B binding to the substrate binding site of FabG-1b and SDR. (**a**) the binding pockets of SDR with epigallocatechin gallate bound. (**b**) the binding pocket of FabG-1b with epigallocatechin gallate bound. (**c**) the binding pockets of SDR with macrolactin B bound. (**d**) the binding pocket of FabG-1b with macrolactin B bound.

anguillarum. Additionally, primers were designed based on the partial amino acid sequence of *V. anguillarum* (which was determined using MALDI-TOF MS/MS) and the conserved regions of the *sdr* genes of *V. cholerae* and *V. alginolyticus* to confirm the *sdr* gene sequence of *V. anguillarum*. The entire ORF sequence of *sdr*, which consists of 759 bp and encodes 252 amino acids on chromosome II, was determined using the DNA-walking method.

The results of this study suggest that FabG-1b, which is responsible for the β-ketoacyl ACP reductase in FASII, and the SDR present on the extra chromosome are likely homologous enzymes. Functional genes related to the FASII system in *V. anguillarum* NB10 were re-established through genome analysis, and FabG-1b and SDR were hypothesized to be paralogous enzymes based on in silico comparative analyses. The amino acid

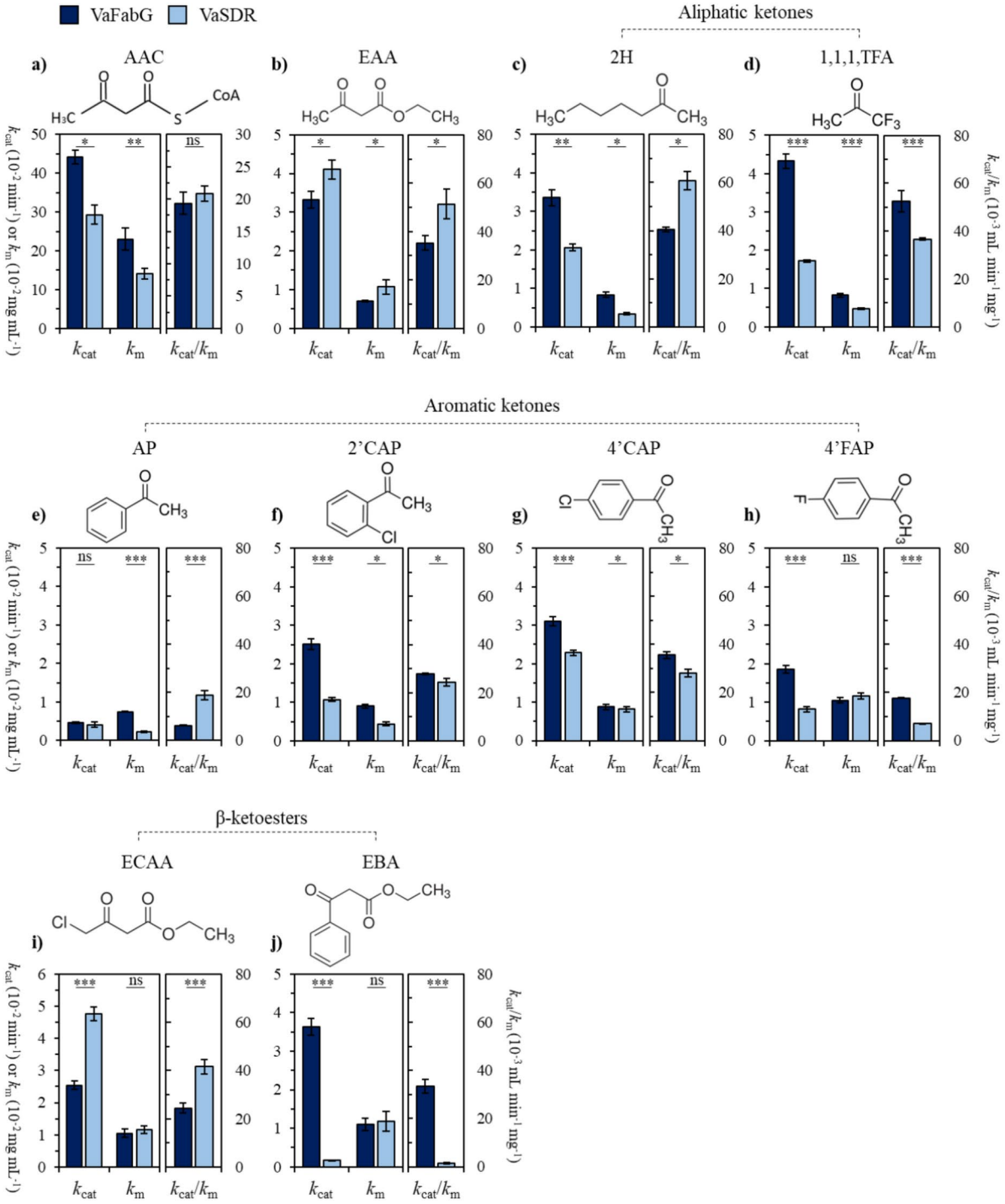

Fig. 5. Kinetic parameters of recombinant FabG-1b and SDR for the 10 tested substrates, (**a**) acetoacetyl coenzyme A (AAC), (**b**) ethyl acetoacetate (EAA), (**c**) 2-heptanone (2H), (**d**) 1,1,1-trifluoroacetone (1,1,1TFA), (**e**) acetophenone (AP), (**f**) 2′-chloroacetophenone (2′CAP), (**g**) 4′-chloroacetophenone (4′CAP), (**h**) 4′-fluoroacetophenone (4′FAP), (**i**) ethyl 4-chloroacetoacetate (ECAA), and (**j**) ethyl benzoylacetate (EBA).

sequence homology between FabG-1b and SDR was only 33.2%; however, the core of functionality, which is the NAD(P)-binding domain and the conserved region of the active site, the topology (predicted using sequence-based homology modelling), and the quaternary homotetramer-type structure showed significant similarity in structure. In particular, the complementary catalytic efficiencies of the two enzymes on various substrates conclusively supported our hypothesis. Among a variety of ketone substrates, FabG-1b exhibited higher specificity toward fluorinated and halogenated aliphatic ketones, aromatic ketones, and aromatic β-ketoesters, whereas SDR could be more specific to non-fluorinated and non-halogenated aliphatic ketones, aromatic ketones,

Bacteria	SDR	Involved in	Note	Method	Ref
V. anguillarum NB10	SDR	fatty acid biosynthesis	Oxidation of various ketone substrates	Recombinant CLA-DH protein	In this study
B. pseudomallei K96243 (Gram -)	BPSS2242	Stress defense (Heat shock)	Down regulation of Hsp70 [1]	Proteomic analysis (2-DE) using △*bpss2242* mutant	68
	BPSS2242	Detoxification (Carbonyl compounds)	Protective system against reactive carbonyl compounds	△*bpss2242* mutant	69
	SDO [2]	Stress defense (Salt)	Relation in enhanced glucose dehydrogenase activity	△*sdo* mutant and complementation	70
C. testosteroni ATCC11996 (Gram -),	SDRx	Metabolism (Hormone)	Degradation of steroids	△*sdrx* mutant and recombinant SDRx protein	71
Lp. plantarum p-8 (Gram +)	CLA-DH [3]	Metabolism (Polyunsaturated fatty acid)	LA [4] conversion into CLA [5]	Recombinant CLA-DH protein	72
Si. meliloti RmP110 (Gram -),	SDR	Metabolism (Carbon uptake)	Carbon utilization deficiency	△*sdr* mutant	73
Sphingomonas sp. A1 (Gram -)	A1-R′	Metabolism (Alginate)	reduction of DEH [6] immediately to detoxify and metabolize alginate	△a*1-r* mutant and recombinant A1-R′ protein	74
St. scabies (Gram +)	SDR	Phytotoxins (CFA-Ile [7])	Reduction in CFA-Ile production	△*sdr* mutant	75

Table 2. Species-specific functions of SDR in a few bacteria. [1] Hsp70; Heat shock protein 70, [2] SDO; short-chain dehydrogenase/oxidoreductase, [3] CLA-DH; conjugated linoleic acids dehydrogenase, [4] LA; linoleic acid, [5] CLA; conjugated linoleic acid, [6] DEH; 4-deoxy-L-erythro-5-hexoseulose uronate, and [7] CFA-Ile; coronafacoyl-L-isoleucine.

and non-aromatic β-ketoesters. The need for β-ketoacyl ACP reductase as a back-up enzyme in *V. anguillarum* NB10 fatty acid biosynthesis could be explained as a survival strategy to rapidly repair cell membrane damage caused by dynamic environmental changes and extreme environmental stress experienced by the bacterium when invading the host. Despite the abundant exogenous supply of lipids and fatty acids from the surrounding environment, utilization of fatty acids in the bacterial FAS-II elongation cycle and lipopolysaccharide synthesis requires ACP-linked substrates, which are supplied only through the intact FAS-II system[64,65]. Therefore, SDR could have been acquired to complement β-ketoacyl ACP reductase activity as a backup enzyme over a long evolutionary period of time. Thus, the two enzymes share a pivotal role in the production of unsaturated fatty acids (UFA) that are essential for surviving and coping with rapid environmental changes. Although we have not validated our inference of the complementary role between FabG-1b and the SDR of *V. anguillarum* NB10 using FabG-deletion mutant strains, a previous study using a FabG-deletion *Campylobacter jejuni* 81–176 strain revealed that FabG plays an essential role in fatty acid membrane integrity[66]. In this study, FabG deletion reduced the ratio of bacterial UFA and chicken colonization of *C. jejuni*, suggesting that FabG may play a pivotal role in UFA production related to bacterial adaptation. Nevertheless, deletion of FabG did not completely inhibit the growth of the strain. This suggests the existence of another homologous enzyme that could indirectly support the role of FabG in fatty acid biosynthesis.

Bacterial SDRs are a very large family of enzymes known as NAD- or NADP-dependent oxidoreductases. Although they are functionally predicted to be highly diverse, little is known about their exact functions[67]. Nevertheless, species-specific functions of SDR have been reported in a few bacteria; SDR in *Burkholderia pseudomallei*, *Comamonas testosteroni*, *Lactiplantibacillus plantarum*, *Streptomyces scabies*, *Sphingomonas* sp., *Sinorhizobium meliloti*, and are directly or indirectly involved in cellular stress defense, detoxification, toxin biosynthesis, and carbohydrate and lipid metabolism (Table 2)[68–75]. Most of these studies used SDR-defective mutant strains; hence, SDR may support a pivotal function in the bacterial life cycle rather than exert a direct effect on bacterial survival. In *V. anguillarum* NB10, SDR functions as a catalyst for the oxidation and reduction of ketones, thereby assisting in the oxidation of fatty acids during the β-oxidation process in metabolic pathways to generate energy. Additionally, it is involved in the biosynthesis of hormones and vitamins, regulates various physiological processes including fatty acid metabolism, steroid metabolism, and amino acid metabolism, and can be cautiously inferred to be directly or indirectly involved in the metabolism of compounds imported from external sources. Furthermore, the coenzyme-binding domains showed significant structural similarity but little sequence identity, suggesting that the structure of the dehydrogenases arose through the genetic fusion of various substrate-specific domains with coenzyme nucleotide sequences from a common ancestor. Therefore, SDR can ultimately ensure stable bacterial survival and growth under extreme environmental stress and contribute to signal transduction, cell protection, and pathogenesis.

Conclusions

In conclusion, we provide evidence that SDR may play a complementary role along with FabG for fatty acid biosynthesis in *V. anguillarum* NB10 as part of a strategy to withstand various stresses in the host and environment. This study acknowledges that all orthologs and paralogs of FABG and SDR within *V. anguillarum*

NB10 could not be investigated due to a lack of foundational scientific information regarding the current protein annotation and experimental evidence for protein functions. Nevertheless, the extensive complementary activity of FabG-1b and SDR against ketone substrates presented in our research, along with the conserved sequences of the active site and NAD(P) binding motif, highlights the importance of simultaneous targeting of paralogous proteins for therapeutic applications as potential antibiotic alternatives. This is particularly relevant considering that these proteins are involved in fatty acid biosynthesis and may serve as alternative targets to address antibiotic resistance. To the best of our knowledge, this study is the first to suggest potential paralog enzymes in *Vibrio*, namely, FabG-1b and SDR. In future studied, we aim to explore the evolution of fatty acid biosynthesis based on omics analysis using mutant strains.

Data availability

Sequence data that support the findings of this study have been already deposited in the National Center for Biotechnology Information with the accession code PRJEB5701. In addition, the datasets used and/or analysed during the current study are available from the corresponding author on reasonable request.

Received: 7 May 2024; Accepted: 3 March 2025
Published online: 13 March 2025

References

1. Loo, K. Y. et al. Incidence of antibiotic resistance in *Vibrio* spp. *Rev. Aquac.* **12**, 2590–2608 (2020).
2. Sampaio, A., Silva, V., Poeta, P. & Aonofriesei, F. Vibrio spp.: Life strategies, ecology, and risks in a changing environment. *Diversity* **14**, 97 (2022).
3. Manchanayake, T., Salleh, A., Amal, M. N. A., Yasin, I. S. M. & Zamri-Saad, M. Pathology and pathogenesis of *Vibrio* infection in fish: A review. *Aquac. Rep.* **28**, 101459 (2022).
4. Ahmed, R., Rafiquzaman, S. M., Hossain, M. T., Lee, J. M. & Kong, I. S. Species-specific detection of *Vibrio alginolyticus* in shellfish and shrimp by real-time PCR using the *groEL* gene. *Aquac. Int.* **24**, 157–170 (2016).
5. Hossain, M. T., Kim, Y. R., Kim, E. Y., Lee, J. M. & Kong, I. S. Detection of *Vibrio cholerae* and *Vibrio vulnificus* by duplex PCR specific to the *groEL* gene. *Fish. Sci.* **79**, 335–340 (2013).
6. Siddique, M. P. et al. *groEL* is a suitable genetic marker for detecting *Vibrio parahaemolyticus* by loop-mediated isothermal amplification assay. *Lett. Appl. Microbiol.* **65**, 106–113 (2017).
7. Austin, B. Vibrios as causal agents of zoonoses. *Vet. Microbiol.* **140**, 310–317 (2010).
8. Sanches-Fernandes, G. M., Sá-Correia, I. & Costa, R. Vibriosis outbreaks in aquaculture: addressing environmental and public health concerns and preventive therapies using gilthead seabream farming as a model system. *Front. Microbiol.* **13**, 904815 (2022).
9. Ma, J. Y. et al. A systematic review, meta-analysis and meta-regression of the global prevalence of foodborne Vibrio spp. infection in fishes: A persistent public health concern. *Mar. Pollut. Bull.* **187**, 114521 (2023).
10. de Souza Valente, C. & Wan, A. H. *Vibrio* and major commercially important vibriosis diseases in decapod crustaceans. *J. Invertebr. Pathol.* **181**, 107527 (2021).
11. Frans, I. et al. *Vibrio anguillarum* as a fish pathogen: virulence factors, diagnosis and prevention. *J. Fish Dis.* **34**, 643–661 (2011).
12. Hasan, M. T. et al. Effects of immunostimulants, prebiotics, probiotics, synbiotics, and potentially immunoreactive feed additives on olive flounder (*Paralichthys olivaceus*): a review. *Rev. Fish. Sci. Aquac.* **27**, 417–437 (2019).
13. Jo, G. A. et al. Isolation and characterization of a 17-kDa FKBP-type peptidyl-prolyl cis/trans isomerase from *Vibrio anguillarum*. *Protein Expr. Purif.* **110**, 130–137 (2015).
14. Kang, D. S., Moon, S. Y., Cho, H. J., Lee, J. M. & Kong, I. S. Interaction of a 22 kDa Peptidyl Prolyl cis/trans Isomerase with the Heat Shock Protein DnaK in *Vibrio anguillarum*. *J. Microbiol. Biotechnol.* **27**, 644–647 (2017).
15. Kim, S. H. et al. Expression, purification and characterization of soluble recombinant peptidyl-prolyl cis/trans isomerase from *Vibrio anguillarum*. *Protein Expr. Purif.* **101**, 54–60 (2014).
16. Oh, R. et al. Cloning and Characterization of Phosphomannomutase/Phosphoglucomutase (pmm/pgm) Gene of *Vibrio anguillarum* Related to Synthesis of LPS. *Microbiol. Biotechnol. Lett.* **44**, 355–362 (2016).
17. Siddique, M. P. et al. Detection of *Vibrio anguillarum* and *Vibrio alginolyticus* by singleplex and duplex loop-mediated isothermal amplification (LAMP) assays targeted to *groEL* and *fklB* genes. *Int. Microbiol.* **22**, 501–509 (2019).
18. Bonnin-Jusserand, M. *et al. Vibrio* species involved in seafood-borne outbreaks (*Vibrio cholerae*, *V. parahaemolyticus* and *V. vulnificus*): Review of microbiological versus recent molecular detection methods in seafood products. *Crit. Rev. Food Sci. Nutr.* **59**, 597–610 (2019).
19. Dicenzo, G. C. & Finan, T. M. The divided bacterial genome: structure, function, and evolution. *Microbiol. Mol. Biol. Rev.* **81**, 10–1128 (2017).
20. Fournes, F., Val, M. E., Skovgaard, O. & Mazel, D. Replicate once per cell cycle: replication control of secondary chromosomes. *Front. Microbiol.* **9**, 1833 (2018).
21. Kirkup, B. C., Chang, L., Chang, S., Gevers, D. & Polz, M. F. *Vibrio* chromosomes share common history. *BMC Microbiol.* **10**, 1–13 (2010).
22. Dowhan, W. Bogdanov, M. & Mileykovskaya, E. Functional roles of lipids in membranes (ed. Vance, D.E. and Vance, J.E.), Biochemistry of Lipids, Lipoproteins and Membranes, 1–37 (Elsevier Press, Amsterdam, 2008)
23. White, S. W., Zheng, J., Zhang, Y. M. & Rock, C. O. The structural biology of type II fatty acid biosynthesis. *Annu. Rev. Biochem.* **74**, 791–831 (2005).
24. Zhang, Y. M. & Rock, C. O. Membrane lipid homeostasis in bacteria. *Nat. Rev. Microbiol.* **6**, 222–233 (2008).
25. Radka, C. D. & Rock, C. O. Mining Fatty Acid Biosynthesis for New Antimicrobials. *Annu. Rev. Microbiol.* **76**, 281–304 (2022).
26. Varakala, S. D., Reshma, R. S., Schnell, R. & Dharmarajan, S. Lead derivatization of ethyl 6-bromo-2-((dimethylamino) methyl)-5-hydroxy-1-phenyl-1H-indole-3-carboxylate and 5-bromo-2-(thiophene-2-carboxamido) benzoic acid as FabG inhibitors targeting ESKAPE pathogens. *Eur. J. Med. Chem.* **228**, 113976 (2022).
27. Vella, P. et al. A FabG inhibitor targeting an allosteric binding site inhibits several orthologs from Gram-negative ESKAPE pathogens. *Bioorg. Med. Chem.* **30**, 115898 (2021).
28. Hu, Z. et al. *Escherichia coli* FabG 3-ketoacyl-ACP reductase proteins lacking the assigned catalytic triad residues are active enzymes. *J. Biol. Chem.* **296**, 100365 (2021).
29. Kim, E. Y., Kim, Y. R., Kim, D. G. & Kong, I. S. A susceptible protein by proteomic analysis from *Vibrio anguillarum* under various environmental conditions. *Bioproc. Biosyst. Eng.* **35**, 273–282 (2012).
30. Holmstrøm, K. & Gram, L. Elucidation of the *Vibrio anguillarum* genetic response to the potential fish probiont *Pseudomonas fluorescens* AH2, using RNA-arbitrarily primed PCR. *J. Bacteriol.* **185**, 831–842 (2003).
31. Lee, J. M. et al. Characterization of salt-tolerant β-glucosidase with increased thermostability under high salinity conditions from Bacillus sp. SJ-10 isolated from jeotgal, a traditional Korean fermented seafood. *Bioproc. Biosyst. Eng.* **38**, 1335–1346 (2015).

32. Holm, K. O., Nilsson, K., Hjerde, E., Willassen, N. P. & Milton, D. L. Complete genome sequence of *Vibrio anguillarum* strain NB10, a virulent isolate from the Gulf of Bothnia. *Stand. Genom. Sci.* **10**, 1–12 (2015).
33. Kanehisa, M. & Goto, S. KEGG: kyoto encyclopedia of genes and genomes. *Nucl. Acids Res.* **28**, 27–30 (2000).
34. Saitou, N. & Nei, M. The neighbor-joining method: a new method for reconstructing phylogenetic trees. *Mol. Biol. Evol.* **4**, 406–425 (1987).
35. Felsenstein, J. Evolutionary trees from DNA sequences: a maximum likelihood approach. *J. Mol. Evol.* **17**, 368–376 (1981).
36. Fitch, W. M. Toward defining the course of evolution: minimum change for a specifc tree topology. *Syst. Biol.* **20**, 406–416 (1971).
37. Jin, C. Z., Lee, J. M., Kim, C. J., Lee, H. G. & Shin, K. S. Genomic Insight into Shimazuella Soli Sp. Nov. Isolated from Soil and Its Putative Novel Class II Lasso Peptide. *Bioeng.* **9**, 812 (2022).
38. Lee, J. M. et al. Improvement of thermostability and halostability of β-1,3–1,4-glucanase by substituting hydrophobic residue for Lys48. *Int. J. Biol. Macromol.* **94**, 594–602 (2017).
39. Waterhouse, A. et al. SWISS-MODEL: homology modelling of protein structures and complexes. *Nucleic Acids Res.* **46**, W296–W303 (2018).
40. Morris, G. M. *et al*. "AutoDock." Automated docking of flexible ligands to receptor-User Guide (2001).
41. Liu, Y. & Cao, Y. Protein–Ligand Blind Docking Using CB-Dock2. In Computational Drug Discovery and Design. 113–125 (New York, NY: Springer US, 2023).
42. Bugnon, M. et al. SwissDock 2024: major enhancements for small-molecule docking with Attracting Cavities and AutoDock Vina. *Nucleic Acids Res.* **52**, W324–W332 (2024).
43. Bradford, M. M. A rapid and sensitive method for the quantitation of microgram quantities of protein utilizing the principle of protein-dye binding. *Anal. Biochem.* **72**, 248–254 (1976).
44. Han, J., Lu, Q., Zhou, L., Liu, H. & Xiang, H. Identification of the polyhydroxyalkanoate (PHA)-specific acetoacetyl coenzyme A reductase among multiple FabG paralogs in *Haloarcula hispanica* and reconstruction of the PHA biosynthetic pathway in *Haloferax volcanii*. *App. Environ. Microbiol.* **75**, 6168–6175 (2009).
45. Zhang, Y. M. & Rock, C. O. Evaluation of epigallocatechin gallate and related plant polyphenols as inhibitors of the FabG and FabI reductases of bacterial type II fatty-acid synthase. *J. Biol. Chem.* **279**, 30994–31001 (2004).
46. Sohn, M.J., Zheng, C.J. &, Kim, W.G. Macrolactin S, a new antibacterial agent with Fab G-inhibitory activity from *Bacillus* sp. AT28. *J. Antibiot*. **61**, 687–691 (2008).
47. Baker, R. E. et al. Infectious disease in an era of global change. *Nat. Rev. Microbiol.* **20**, 193–205 (2022).
48. Kim, J.H. *et al*. Efficient production of poly γ-d-glutamic acid from the bloom-forming green macroalgae, *Ulva* sp., by *Bacillus* sp. SJ-10. *Biotechnol. Bioeng.* **116**, 1594–1603 (2019).
49. Brumfield, K. D. et al. Environmental parameters associated with incidence and transmission of pathogenic *Vibrio* spp. *Environ. Microbiol.* **23**, 7314–7340 (2021).
50. Semenza, J. C. Cascading risks of waterborne diseases from climate change. *Nat. Immunol.* **21**, 484–487 (2020).
51. Andree, K. B., Carrasco, N., Carella, F., Furones, D. & Prado, P. *Vibrio mediterranei*, a potential emerging pathogen of marine fauna: investigation of pathogenicity using a bacterial challenge in *Pinna nobilis* and development of a species-specific PCR. *J. App. Microbiol.* **130**, 617–631 (2021).
52. Baker-Austin, C., Trinanes, J., Gonzalez-Escalona, N. & Martinez-Urtaza, J. Non-cholera vibrios: the microbial barometer of climate change. *Trends Microbiol.* **25**, 76–84 (2017).
53. Ballal, M., Shetty, V., Bangera, S. R., Prabhu, M. & Umakanth, S. *Vibrio furnissii*, an emerging pathogen causing acute gastroenteritis: a Case Report. *JMM. Case. Rep.* **4**, e005111 (2017).
54. Chen, X. et al. Responses of free-living *vibrio* community to seasonal environmental variation in a Subtropical Inland Bay. *Front. Microbiol.* **11**, 610974 (2020).
55. Kimes, N. E. et al. Temperature regulation of virulence factors in the pathogen *Vibrio coralliilyticus*. *ISME. J.* **6**, 835–846 (2012).
56. Kumar, S. et al. Delineating virulence of *Vibrio campbellii*: a predominant luminescent bacterial pathogen in Indian shrimp hatcheries. *Sci. Rep.* **11**, 15831 (2021).
57. Kunitomo, K., Uemura, N., Shimizu, T., Hayano, S. & Tsuji, T. Skin and soft tissue infections and bacteremia caused by *Vibrio cincinnatiensis*. *IDCases.* **29**, e01564 (2022).
58. Padovan, A. et al. Occurrence and dynamics of potentially pathogenic vibrios in the wet-dry tropics of northern Australia. *Mar. Environ. Res.* **169**, 105405 (2021).
59. Sheahan, M. et al. Examining the relationship between climate change and vibriosis in the United States: projected health and economic impacts for the 21st century. *Environ. Health Perspect.* **130**, 087007 (2022).
60. Jones, E. H. et al. *Vibrio* infections and surveillance in Maryland, 2002–2008. *Public Health Rep.* **128**, 537–545 (2013).
61. Xie, J. et al. Outbreak of vibriosis caused by *Vibrio harveyi* and *Vibrio alginolyticus* in farmed seahorse *Hippocampus kuda* in China. *Aquac.* **523**, 735168 (2020).
62. Igbinosa, E. O. & Okoh, A. I. *Vibrio fluvialis*: an unusual enteric pathogen of increasing public health concern. *Int. J. Environ. Res. Public Health* **7**, 3628–3643 (2010).
63. Hutchins, D. A. et al. Climate change microbiology—problems and perspectives. *Nat. Rev. Microbiol.* **17**, 391–396 (2019).
64. Morvan, C. et al. The Staphylococcus aureus FASII bypass escape route from FASII inhibitors. *Biochimie.* **141**, 40–46 (2017).
65. Yao, J. & Rock, C. O. Exogenous fatty acid metabolism in bacteria. *Biochimie.* **141**, 30–39 (2017).
66. Asakura, H. et al. Ex vivo proteomics of *Campylobacter jejuni* 81–176 reveal that FabG affects fatty acid composition to alter bacterial growth fitness in the chicken gut. *Res. Microbiol.* **167**, 63–71 (2016).
67. Kallberg, Y., Oppermann, U., Jörnvall, H. & Persson, B. Short-chain dehydrogenases/reductases (SDRs) Coenzyme-based functional assignments in completed genomes. *Eur. J. Biochem.* **269**, 4409–4417 (2002).
68. Reamtong, O. et al. Altered proteome of a *Burkholderia pseudomallei* mutant defective in short-chain dehydrogenase affects cell adhesion, biofilm formation and heat stress tolerance. *PeerJ.* **8**, e8659 (2020).
69. Chamchoy, K. et al. Functional analysis of BPSS2242 reveals its detoxification role in *Burkholderia pseudomallei* under salt stress. *Sci. Rep.* **10**, 10453 (2020).
70. Pumirat, P. *et al*. The role of short-chain dehydrogenase/oxidoreductase, induced by salt stress, on host interaction of *B. pseudomallei*. *BMC Microbiol.* **14**, 1–11 (2014).
71. Liu, C., Liu, K., Zhao, C., Gong, P. & Yu, Y. The characterization of a short chain dehydrogenase/reductase (SDRx) in *Comamonas testosteroni*. *Toxicol. Rep.* **7**, 460–467 (2020).
72. Zhao, W. *et al*. Characterization and functional of four mutants of hydroxy fatty acid dehydrogenase from *Lactobacillus plantarum* p-8. *FEMS Microbiol. Lett.* **369**, fnac060 (2022).
73. Jacob, A. I. et al. Mutational analysis of the *Sinorhizobium meliloti* short-chain dehydrogenase/reductase family reveals substantial contribution to symbiosis and catabolic diversity. *Mol. Plant-Microbe. Interact.* **21**, 979–987 (2008).
74. Takase, R., Mikami, B., Kawai, S., Murata, K. & Hashimoto, W. Structure-based conversion of the coenzyme requirement of a short-chain dehydrogenase/reductase involved in bacterial alginate metabolism. *J. Biol. Chem.* **289**, 33198–33214 (2014).
75. Bown, L., Altowairish, M. S., Fyans, J. K. & Bignell, D. R. Production of the *Streptomyces scabies* coronafacoyl phytotoxins involves a novel biosynthetic pathway with an F420-dependent oxidoreductase and a short-chain dehydrogenase/reductase. *Mol. Microbiol.* **101**, 122–135 (2016).

Acknowledgements
This research was supported by the National Institute of Fisheries Science, Ministry of Oceans and Fisheries, Korea (R2025051).

Author contributions
D.-G.K., S.Y.P., S.M.R., and J.M.L. performed the experiments, analyzed the data, and wrote the original manuscript. D.-G.K., and J.M.L. obtained funding and contributed to the study design. D.-G.K., S.M.R., and J.M.L. analyzed the data and wrote and revised the manuscript. D.-G.K., S.Y.P., S.M.R., and J.M.L. participated in the discussion of the results. All authors read and approved the final manuscript.

Declarations

Competing interests
The authors declare no competing interests.

Additional information
Supplementary Information The online version contains supplementary material available at https://doi.org/10.1038/s41598-025-92645-x.

Correspondence and requests for materials should be addressed to J.M.L.

Reprints and permissions information is available at www.nature.com/reprints.

Publisher's note Springer Nature remains neutral with regard to jurisdictional claims in published maps and institutional affiliations.